Research Article | Vol. 28, No. 23 / 9 November 2020 / Optics Express 34079

Optics EXPRESS

Dual-channel optical switch, refractive index sensor and slow light device based on a graphene metasurface

XINPENG JIANG, DINGBO CHEN, ZHAOJIAN ZHANG, JIE HUANG, KUI WEN, JIE HE, AND JUNBO YANG*

Center of Material Science, College of Liberal Arts and Sciences, National University of Defense Technology, Changsha 410073, China

*yangjunbo@nudt.edu.cn

Abstract: In this paper, we propose a graphene-based metasurface that exhibits multifunctions including tunable filter and slow-light which result from surface plasmon polaritons (SPPs) of graphene and plasmon induced transparency (PIT), respectively. The proposed metasurface is composed by two pairs of graphene nano-rings and a graphene nanoribbon. Each group of graphene rings is separately placed on both sides of the graphene nanoribbon. Adjusting the working state of the nanoribbon can realize the functional conversion of the proposed multifunctional metasurface. After that, in the state of two narrow filters, we put forward the application concept of dual-channel optical switch. Using phase modulation of PIT and flexible Fermi level of graphene, we can achieve tunable slow light. In addition, the result shows that the graphene-based metasurface as a refractive index sensor can achieve a sensitivity of 13670 nm/RIU in terahertz range. These results enable the proposed device to be widely applied in tunable optical switches, slow light, and sensors.

1. Introduction

The plasmon induced transparency (PIT), a plasmonic analogue of the electromagnetic induced transparency (EIT), produces a narrow spectral window of transmission near an absorption peak excited by surface plasmon polaritons (SPPs) [1–3]. The generation of PIT is generally attributed to the coupling of bright and dark modes which can be grouped into two main categories according to the production mechanism: (1) Through the coupling between two bright modes, a transparent window is generated between the two bright fields [4,5]. (2) The coupling between dark and bright mode for which the purpose is to reach a transparent window in the original frequency range of SPPs [6–10].

The superior characteristics of SPPs are not limited to PIT. SPPs are surface electromagnetic waves formed by collective oscillation of free electrons in metal interacting with the incident light field. SPPs, which include waveguide plasmon polaritons and surface plasmon resonance (SPR), could support a series of functional devices, such as color-tunable and perfect absorber [11–13]. Because of the enhanced optical transmission (EOT) phenomenon of SPPs, it can be used for filter and absorber [14–16]. However, the tune of metal SPPs mainly depends on the change of structure scale, which is difficult to achieve in the fabrication.

As a two-dimensional material, graphene attracts considerable attention of researchers because of its unique optoelectronic properties [17–21]. Due to the semi-metallic properties of graphene, single-layer graphene can be processed into ribbon [22,23], disks [24,25], and split rings [26,27] that can also excite SPPs. The SPPs properties of graphene can be controlled by the Fermi level of graphene. According to some reports [28,29], the Fermi level of graphene can be flexibly tuned by the gate voltage. Graphene, as a platform to replace metals to excite PIT, has produced a series of applications, such as sensors [30–32], absorbers [33–36] and slow light [37,38]. Similarly, the

#412442
Journal © 2020

https://doi.org/10.1364/OE.412442
Received 13 Oct 2020; accepted 17 Oct 2020; published 26 Oct 2020

use of graphene SPPs can achieve efficient narrow-band filter, and this filter can dynamically tune the response frequency [39–41]. Besides, both surface plasmon filter and PIT can be used for refractive index sensing applications [42,43] with high sensitivity. However, there are rarely related reports on multifunctional devices that combine filters with PIT.

In this paper, we proposed a graphene-based metasurface that exhibits multifunction including tunable filter and PIT which can achieve function switch by applying an external voltage. The proposed metasurface is composed by four graphene nano-rings and a graphene nanoribbon which generate the bright and dark mode on the SiO_2-Si substrate. An ion-gel layer and a conductive layer are attached to the metasurface, and an Au gate is manufactured on the ion-gel layer. By changing the gate voltage, we can independently tune the Fermi level of graphene rings and nanoribbons. The simulation result of finite-difference time-domain (FDTD) show that the proposed metasurface has some excellent properties including two narrow filters, tunable slow light of PIT and high refractive index sensitivity of 136700 nm/RIU in the terahertz. Based on the behavior of two tunable filters, we propose a concept of dual-channel optical switch which including four states by tuning the Fermi level of graphene. With the above benefits, the proposed device is potential in tunable optical switches, slow light, and sensors.

2. Model construction

Figure 1 exhibits the graphene-based multifunction device, which is composed of periodically patterned graphene single layer sitting on the SiO_2-Si substrate. The thickness of SiO_2 and Si are both 0.1μm, the relative permittivity is 1.96 and 11.7, respectively. The 3D FDTD method is used for the numerical simulation and the commercial software of Lumerical FDTD Solutions is employed. In our simulation, the thickness of the graphene layer is 1 nm. The graphene-based metasurface unit consists of a continuous nanoribbon and four rings with the same outer diameter. Among them, in order to exist a dark mode, we set up continuous nanoribbon with width of 0.8μm. The continuous nanoribbon is in the middle of the periodic unit. The four graphene rings are named as *R1, R2, R3* and *R4*, which are marked in Fig. 1(b). The four rings are divided into two groups which are named as *G1* and *G2* (*R1* and *R2* are *G1*, *R3* and *R4* are *G2*). The rings of each group have the same scale and are symmetrical about the Y axis. The ion-gel and conductive layer, described by a nondispersive permittivity $\varepsilon=1.82$ [44], are attached to the top of the entire structure. The voltage is tuned by the Au gate fabricated on the ion-gel layer, thereby tuning the Fermi energy level of the graphene metasurface. Since the ion-gel layer has little effect on the output spectrum and phase modulation of the entire structure, it is omitted in the simulation. This part of the content is reflected in the *Supplementary S1*. Moreover, the boundary condition of x direction is symmetrical layer, y direction is periodic layer, and z direction is perfectly matched layers (PML).

THz plane waves are normally illuminated on the device and the monitors to obtain transmission spectrum $T(\omega)$ and phase change $\psi(\omega)$. Due to the SPPs of graphene, the transmission spectrum and phase exist some changes, which can be explained by the Kubo formula to the conductivity $\sigma(\omega)$ of graphene [45,46]:

$$\sigma(\omega) = \sigma_{\mathrm{intra}}(\omega) + \sigma_{\mathrm{inter}}(\omega), \tag{1}$$

$$\sigma_{\mathrm{intra}}(\omega) = \frac{2e^2 k_B T}{\pi\hbar^2}\frac{i}{\omega + i/\tau}\ln\left[2\cosh\left(\frac{E_f}{2k_B T}\right)\right], \tag{2}$$

$$\sigma_{\mathrm{inter}}(\omega) = \frac{e^2}{4\hbar^2}\left[\frac{1}{2} + \frac{1}{\pi}\arctan\left(\frac{\hbar\omega - 2E_f}{2k_B T}\right) - \frac{i}{2\pi}\ln\frac{(\hbar\omega + 2E_f)^2}{(\hbar\omega - 2E_f)^2 + 4(k_B T)^2}\right]. \tag{3}$$

Where ω is response frequency of graphene SPPs, E_f is the chemical potential (Fermi level), e is the elementary charge. Both k_B and $\hbar$ are constants which represent Boltzmann constant and Planck constant respectively. T represents the ambient temperature which we set 300K

Research Article Vol. 28, No. 23 / 9 November 2020 / Optics Express 34081

Optics EXPRESS

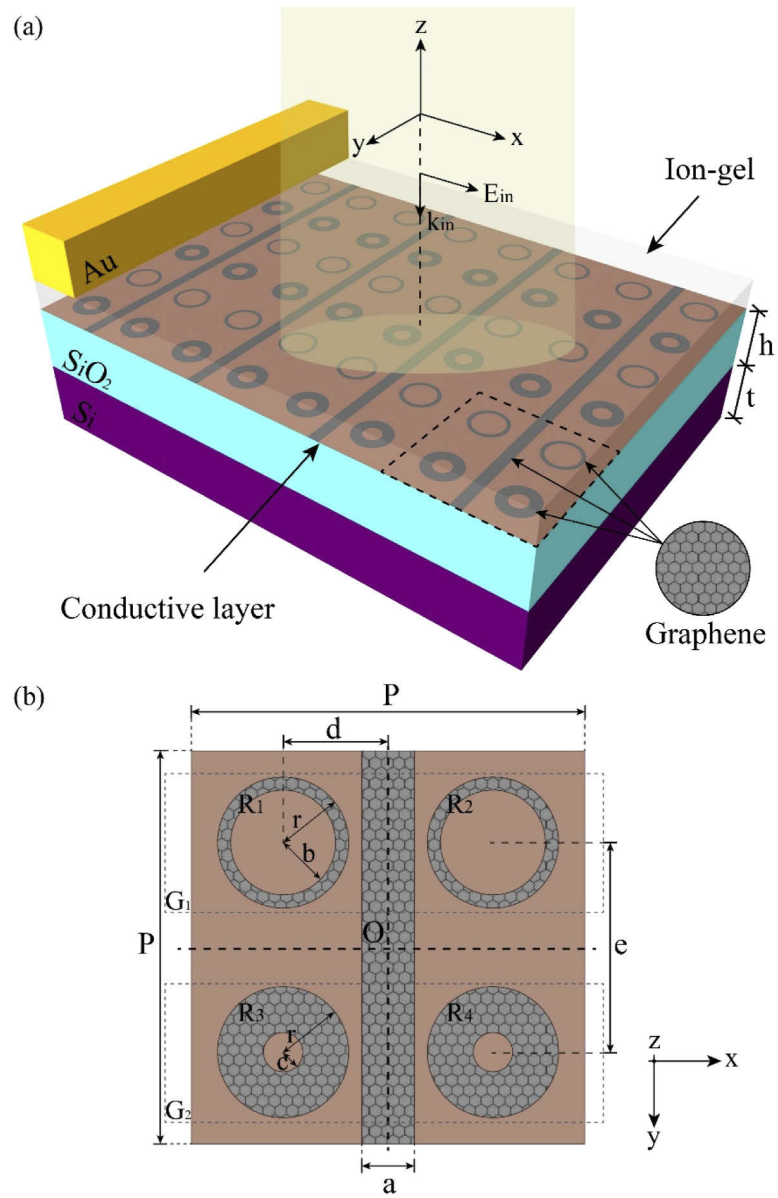

Fig. 1. (a) Schematic of the proposed multifunctional graphene metasurface consisting of two pairs of graphene nano-rings and a graphene nanoribbon sitting on the SiO_2-Si substrate. The thickness of SiO_2 and Si are *h=0.1*μ*m, t=0.1*μ*m*. The ion-gel was spin-coated on the graphene metasurface and contacted to the Au electrodes as the top gate. An ultrathin and transparent conduct thin layer was deposited between the SiO_2 and graphene as the bottom gate. (b) Top view of unit cell of the structure in Fig. 1(a) with its geometrical parameters: *P=6*μ*m, r=1.0*μ*m, a=0.8*μ*m, b=0.8*μ*m, c=0.3*μ*m, d=1.6*μ*m, e=3.2*μ*m*. Names and groups of graphene rings are marked on the graph. (*R1* and *R2* are *G1*, *R3* and *R4* are *G2*).

Optics EXPRESS

to make it close to reality in the simulation. τ is the time of carrier relaxation, which can be given by $\tau = \mu E_f/(ev_F^2)$, thereby $v_F = 10^6 m \cdot s^{-1}$ expresses Fermi velocity [47,48]. When the $E_f \gg (\hbar\omega, k_B T)$, we can use the metal-like Drude model to simplify the above equation in terahertz band as [49]:

$$\sigma(\omega) = \frac{eE_f}{\pi\hbar^2} \frac{i}{\left(\omega + \frac{i}{\tau}\right)}. \tag{4}$$

The graphene Fermi level can be changed by gate voltage and chemical surface modification. This change essentially changes the doping level of graphene n_s, and the relationship between E_f and n_s can be given by the following equation:

$$E_f = \hbar v_F \sqrt{\pi n_s}. \tag{5}$$

Where the $v_F = 10^6 m \cdot s^{-1}$ expresses Fermi velocity, it also set in our simulation. Based on simple capacitor model, we can give the linear dependence on the n_s and the gate voltage [50]:

$$n_s = \frac{\varepsilon_r \varepsilon_0 |V_g - V_{dirac}|}{ed}. \tag{6}$$

Where ε_r and ε_0 represent the permittivity of insulator layer and vacuum, respectively. $|V_g - V_{Dirac}|$ is the applied voltage, d is the thickness of insulator layer. According to the above equation, we can make a conclusion of the SPPs response wavelength λ:

$$\lambda = \frac{2\pi\hbar c}{e} \sqrt{\frac{\omega \varepsilon_r \varepsilon_0}{E_f}}. \tag{7}$$

We use the Au gate bias voltage to change the working state of the graphene nanoribbons. According to the previous reports [26,40], we can know that there is almost no SPPs when the Fermi level of the graphene layer is 0. Since the graphene nanoribbons are off (Fermi level is 0) and the Fermi level of graphene rings are 1eV, the simulation results of the proposed device show two narrow filters which excited by the SPPs of graphene rings in the terahertz as shown in Fig. 2(a). Figure 2(a) displays the transmission spectrum for different states under the plane wave incident to single-group of graphene rings and double-group of graphene rings. According to the transmission spectrum of different states, we can make a conclusion that the coupling between the two narrow filters is weak. It reminds us of its potential to apply in switch. Figure 2(b) shows two narrow filters which depend on the graphene Fermi level are tunable. It is worth noting that when the Fermi level of graphene decreases, the transmission spectrum of the proposed device undergoes a significant blue shift. This phenomenon is consistent with the tunable conductivity theory of graphene mentioned above. Through Fermi level tuning, we realize dual-band tunable filters.

We also add the graphene nanoribbon coupling a dark mode to generate the transparent window in two original narrow filters. When we turn on the graphene nanoribbon (Fermi level of graphene nanoribbon is 1eV), we can get two PIT windows at 5.16THz and 9.18THz, as shown in Fig. 3(a). The incident wave causes the graphene to excite the surface SPPs, as a result, the transmission trough emerges in the spectrum. This mode is named as *bright mode (B)* as shown in the blue line. The *dark mode (D)* has no response frequency to the incident wave due to the continuity of the nanoribbons, as shown in the green line. Only when the bright mode and the dark mode exist at the same time, because of the destructive interference between dark mode and bright mode, the bright and dark mode produce the transparent window as shown in the red line. We also give the electric field distribution at the transparent window frequency and the transmission trough frequency. In addition, in order to study the formation of the transparent window, we have also given the electric field distribution in the mode with only SPPs as shown in Fig. 3(c). Through Fig. 3(a), we can find that the transparent window of *G1* and the nanoribbon is easier to

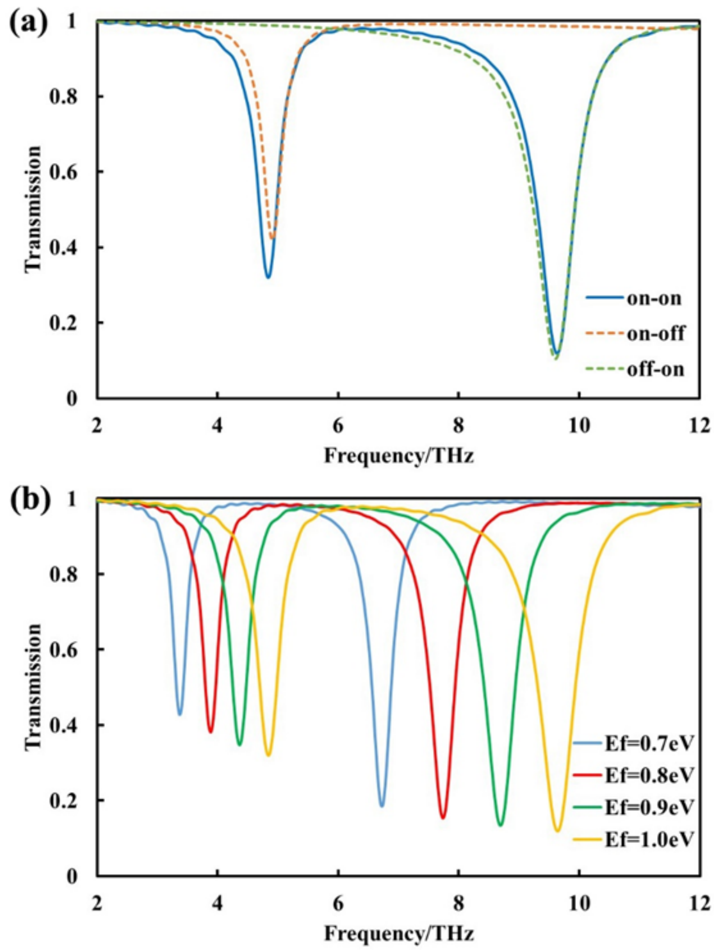

Fig. 2. (a) The transmission spectra of two tunable narrow filters with different states of the graphene metasurface. (The off state indicates that the Fermi level of single-group of graphene rings is 1.0 eV, and the on state indicates that the Fermi level is 0 eV. For example, "off-off" means that both *G1* and *G2* are 1 eV) (b) The response of two tunable narrow filters with different Fermi energies of graphene. (A color version of this figure can be viewed online.)

observe. This phenomenon can be reasonably explained by CMT [37,51,52]. Figure 3(b) shows the coupling between the bright and dark modes by CMT. Two states of resonances are named as m_B and m_D respectively describe the resonance excited by SPPs and the resonance of the coupling between bright mode and dark mode, where the superscript "*out*" and "*in*" represent the input and output in the resonance, and the subscript "+" and "-" describe the direction of the mode transmission. Thus, the system can be expressed as:

$$\begin{pmatrix} \gamma_B & -i\kappa_{BD} \\ -i\kappa_{DB} & \gamma_D \end{pmatrix} \cdot \begin{pmatrix} m_B \\ m_D \end{pmatrix} = \begin{pmatrix} -\tau_{eB}^{-\frac{1}{2}} & 0 \\ 0 & -\tau_{eD}^{-\frac{1}{2}} \end{pmatrix} \cdot \begin{pmatrix} B_+^{in} + B_-^{in} \\ D_+^{in} + D_-^{in} \end{pmatrix}. \tag{8}$$

Where κ_{BD} and κ_{DB} represent the coupling coefficient between bright mode and dark mode,

Optics EXPRESS

respectively. Moreover, ω is the angular frequency of the incident waves, $\gamma_{iB(D)} = \frac{1}{\tau_{iB(D)}}$ express the decay rate due to intrinsic loss, $\gamma_{eB(D)} = \frac{1}{\tau_{eB(D)}}$ express the attenuation rate of energy that escaping from mode to outer space. According to Eq. (8) and $\gamma_{iB(D)}$ and $\gamma_{eB(D)}$, we can get

$$\gamma_B = i\omega - i\omega_B - \gamma_{iB} - \gamma_{eB}, \tag{9}$$

$$\gamma_D = i\omega - i\omega_D - \gamma_{iD} - \gamma_{eD}. \tag{10}$$

Supported by the principle of conservation of energy, the input and output of the bright and dark modes are expressed as follows,

$$D_+^{in} = B_+^{out} e^{i\phi}, B_-^{in} = D_-^{out} e^{i\phi}, \tag{11}$$

$$B_\pm^{out} = B_\pm^{in} - \tau_{eB}^{-\frac{1}{2}} m_B, D_\pm^{out} = D_\pm^{in} - \tau_{eD}^{-\frac{1}{2}} m_D. \tag{12}$$

Here, $e^{i\phi}$ expresses the phase shift of the incident wave. According to Eqs. (8)-(12) and the initial condition that only single incident wave is incident on the graphene layer from the negative direction of the z-axis, it means that $D_-^{in} = 0$. The transmission coefficient of the system can be

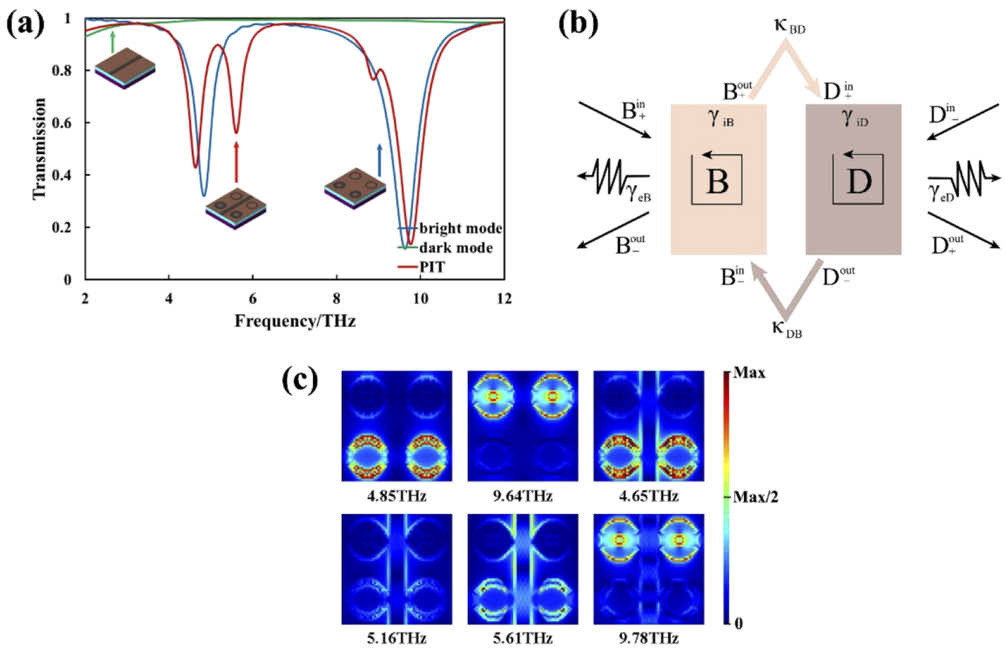

Fig. 3. (a) The function translation of graphene metasurface by tuning the graphene nanoribbon. (A color version of this figure can be viewed online.) (b) Equivalent CMT model between bright mode and dark mode for the proposed structure in this work. (c) Simulated electric field intensities profile with different states of graphene metasurface. Two SPPs response frequencies of the narrow filter at 4.85THz and 9.64THz are shown in turn. Comparing the resonance of narrow filters, transmission peak (transparent window at 5.16THz) and three resonance dips (4.65THz, 5.61THz and 9.78THz) are significantly different.

Optics EXPRESS

quantitatively expressed as

$$t = \frac{D_+^{out}}{B_+^{in}} = e^{i\phi} + \Big[\tau_{eB}^{-1}\gamma_D e^{i\phi} + \tau_{eD}^{-1} e^{i\phi}\gamma_B + (\tau_{eB}\tau_{eD})^{-\frac{1}{2}} e^{2i\phi}\chi_B \\ +(\tau_{eB}\tau_{eD})^{-\frac{1}{2}}\chi_D\Big] \cdot (\gamma_B\gamma_D - \chi_B\chi_D)^{-1}. \tag{13}$$

Where $\chi_{B(D)} = i\kappa_{DB(BD)} + 2\sqrt{\gamma_{eB}\gamma_{eD}} \cdot e^{i\phi}$, and we can make a conclusion that $T = |t|^2$.

In addition, the coupling of *G2* and graphene nanoribbon also has a PIT phenomenon. When we test *G2* separately, we can see the existence of this PIT phenomenon. However, due to the mutual influence between the two-ring systems, the PIT becomes more difficult to observe than before. This part of the work is detailed in *Supplementary S2*.

3. Result and discussion

According to the CMT theory, we specifically discussed the PIT peak generated by *G1* and continuous nanoribbon. The transmission spectrum of the FDTD simulation and the curve fitting CMT theory are compared when the Fermi level of *G1* changes from 0.8 eV to 1.0 eV. As shown in Fig. 4, the blue dotted line dedicates the FDTD simulation result, and the red solid line shows the curve fitting CMT theory. Combining with the coupled-mode theory and the theoretical conclusions, which are explained in Eqs. (8)-(13), we get the transmission spectrum given by CMT fitting curve. Comparing the two curves, we can see that the results of the CMT are consistent with the results obtained from the FDTD simulation. In addition, we found that the PIT generated by *G1* and continuous nanoribbon is consistent with the tunable conductivity theory of graphene. As the Fermi level increases, the two dips undergo a blue shift. In the above, we have discussed the proposed graphene dual-band tunable filter using the graphene conductivity adjustable theory. Here, the two dips based on the PIT effect of graphene can also be explained by the theory of tunable graphene conductivity.

Detecting refractive index is an indispensable method which is widely used in biochemical molecular sensing applications [43,53] and solution salinity detections [54]. To investigate the refractive index sensitivity of the SPP excited by graphene, we change the refractive index of the top surrounding medium and track the change of the response wavelength of the SPP resonance center. All the structural parameters and the Fermi level setting of the graphene metasurface are consistent with the initial state of the tunable filter. (The Fermi level of graphene rings are 1eV and nanoribbon is 0eV.) The sensitivity of the device depends on the relationship between the change in refractive index and the change in resonance wavelength, which can be expressed as [55,56]:

$$S = \frac{d\lambda}{dn}, \tag{14}$$

$$FOM = \frac{S}{FWHM}. \tag{15}$$

Where $d\lambda$ represents the shift of resonance center wavelength, dn is the change of refractive index. *FWHM* is the full width at half maximum of the transparency window. As shown in Fig. 5(a), we can find that as the refractive index increases, the resonance peak has a red shift. As for *FOM*, the resonance generated by *G2* is more obvious than the resonance generated by *G1*. The calculated sensitivity of the resonance of *G2* is 13670 nm/RIU, *FOM* is 6. When the refractive index changes from 1.0 to 1.3, the resonance wavelength is red-shifted from 31.11μm to 35.22μm. Compared with the previously reported work [40,55,56], the sensitivity of the proposed device is high in the terahertz. Figure 5(b) shows that the linearity of the proposed structure sensitivity which is crucial to evaluate the quality of the sensor. Besides, we compared the work of others to illustrate that our device is highly sensitive to the refractive index, as shown in Table 1.

Optics EXPRESS

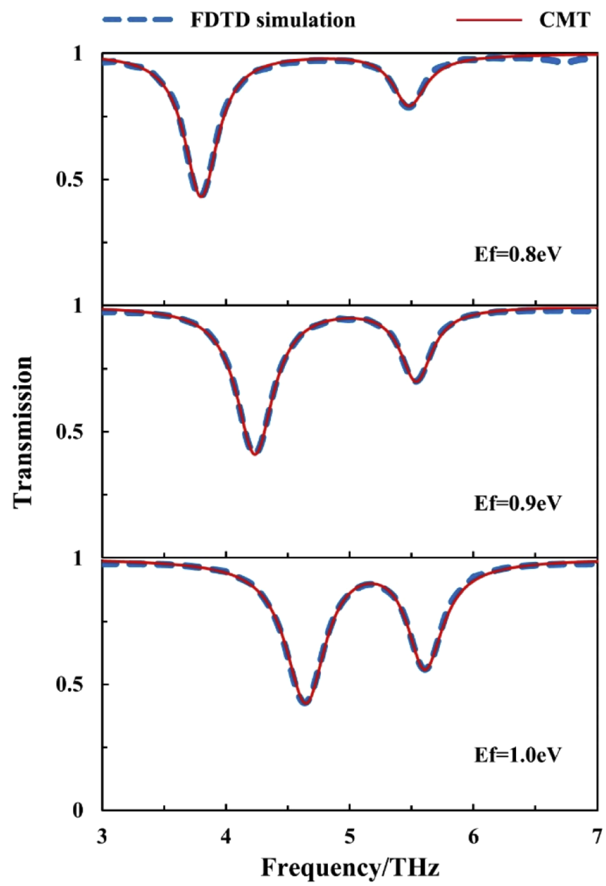

Fig. 4. The transmission spectra of the *G1* graphene PIT metamaterial at terahertz band when E_f in mode *D* (graphene nanoribbon) and *G2* is maintained at 1.0 eV and in element *B* (*G1*) is 0.8 eV, 0.9 eV, 1.0 eV, from top to bottom.

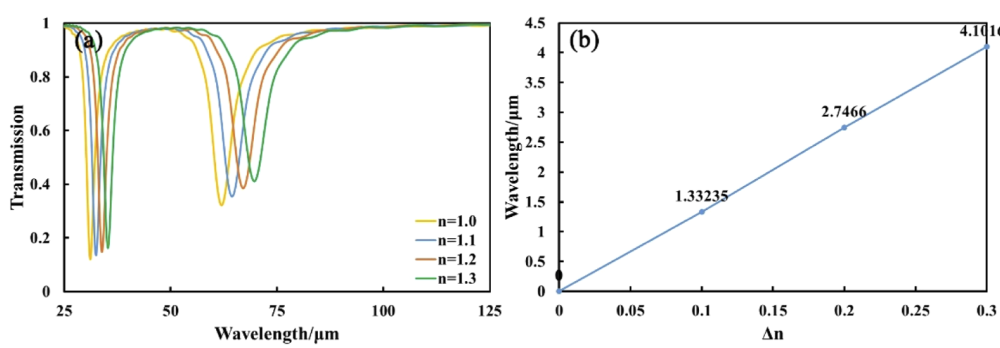

Fig. 5. (a) Simulated transmittance spectra of the metamaterial with refractive index ranging from 1 to 1.3. (A color version of this figure can be viewed online.) (b) Wavelength change of the tunable filter peak versus the refractive index (blue solid line with the marked wavelength).

Optics EXPRESS

Table 1. Comparison of sensitivity and tunability of the graphene metasurface with other sensitive refractive index sensors.

Ref.	[57]	[42]	[58]	Our metasurface
Sensitivity (nm/RIU)	590	3020	5160	13670
Tunability	No	Yes	Yes	Yes

Similarly, when the graphene nanoribbon is in the "off" state, we can get the dual-channel optical switch. According to the characteristics of the proposed device that the two transmission troughs have a certain distance during the filtering process and the coupling between the two transmission dips is weak, we propose the design concept of a dual-channel optical switch in the terahertz. This switch has four states (on-on, on-off, off-on, off-off), and the four states can be quickly converted by tuning the graphene Fermi levels of two groups *G1* and *G2* including *R1, R2, R3* and *R4*. The Fermi level of the graphene ring group (*G1* and *G2*) is 1 or 0, indicating the "on" state and "off" state, respectively. Four states are clearly described in Table 2, including the Fermi levels of different groups of graphene rings and the corresponding transmission spectrum. Figures 6(a)–6(d) illustrate transmission spectrum under different states, which can be flexibly converted.

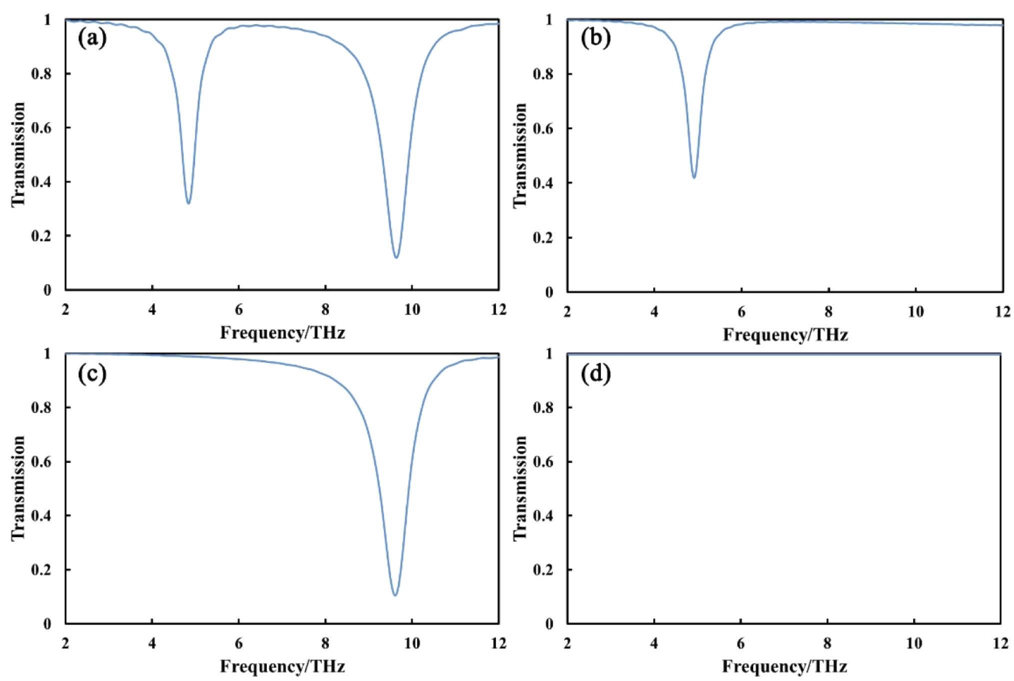

Fig. 6. (a) The transmission spectra with different Fermi levels for different groups of graphene rings (G1 and G2) at four states: (a) with 1 eV and 1 eV, respectively, (b) with 1 eV and 0 eV, respectively, (c) with 0 eV and 1 eV, respectively, and (d) with 0 eV and 0 eV, respectively.

Finally, we discuss the effect of the device on slow light in the case of an induced transparent window, especially the phase change near the transparent window caused by the coupling of *R1, R2* and graphene nanoribbon light-dark mode. The narrow-spectrum resonance effect is one of the methods to realize slow light. The narrow resonant peak implies that the effective refractive index of the nearby wavelength changes drastically, so it has a strong dispersion effect, and strong

Optics EXPRESS

Table 2. Four states of dual-channel optical switches and different chemical potentials.

State	Fermi level (eV)	Figure
on-on	1 1	(a)
on-off	1 0	(b)
off-on	0 1	(c)
off-off	0 0	(d)

dispersion will cause the speed of the light wave group to delay and form slow light. PIT is a typical narrow-spectrum resonance. The delay time of the slow light effect can be calculated by the following formula [59]:

$$\tau_g = \frac{d\psi(\omega)}{d\omega}. \tag{16}$$

Where $\psi(\omega)$ represents the phase difference of light of different frequencies from the incident end to the exit end of the common waveguide. As shown in Fig. 7(a), we can find that different Fermi level of *G1* can tune the response frequency of PIT. This change is consistent with the tunable conductivity theory of graphene. Figures 7(b)–7(d) illustrate the phase shift of PIT when the Fermi level of *G1* increases. According to the phase shift, we can clearly get the delay time near the transparent window which can be varied by the Fermi level changing. When $E_f = 0.8eV$, the delay time reaches a maximum at the induced transparent window, and the value is up to 0.227ps. We can find that the range of slow light can be dynamically adjusted by the Fermi level, which offers a novel idea for designing applications with high-performance slow-light index in the future.

In order to reflect the versatility of the proposed device, we compared the proposed device with other devices [60–62] which realize some unique functions. As shown in Table 3, the proposed device in our work has some functions including dual-channel optical switch, sensitive refractive index sensor and slow light. All of the above devices have the function of an optical switch. However, the previous works are based on the coupling of bright and dark modes to realize optical switches. The proposed device can not only realize the optical switch through PIT, but also realize the dual-channel optical switch with four states by using graphene SPPs. Besides, our metasurface has a competitive sensitivity of refractive index with the recent study [60,62]. Compared with the previous reports [61,62], the slow light efficiency of our metasurface still needs to improve. However, it is worth mentioning that a device with such comprehensive functions and unique sensitivity of refractive index is rarely reported in previous reports.

Table 3. Comparison of the function of the graphene metasurface with other graphene devices.

Ref.	Mode number of optical switch	Sensitivity of refractive index (nm/RIU)	Slow light (ps)
Our metasurface	Four modes	136700	0.227
[60]	Two modes	2300	Do not mention
[61]	Two modes	Do not mention	0.7
[62]	Two modes	4310	1.33

Optics EXPRESS

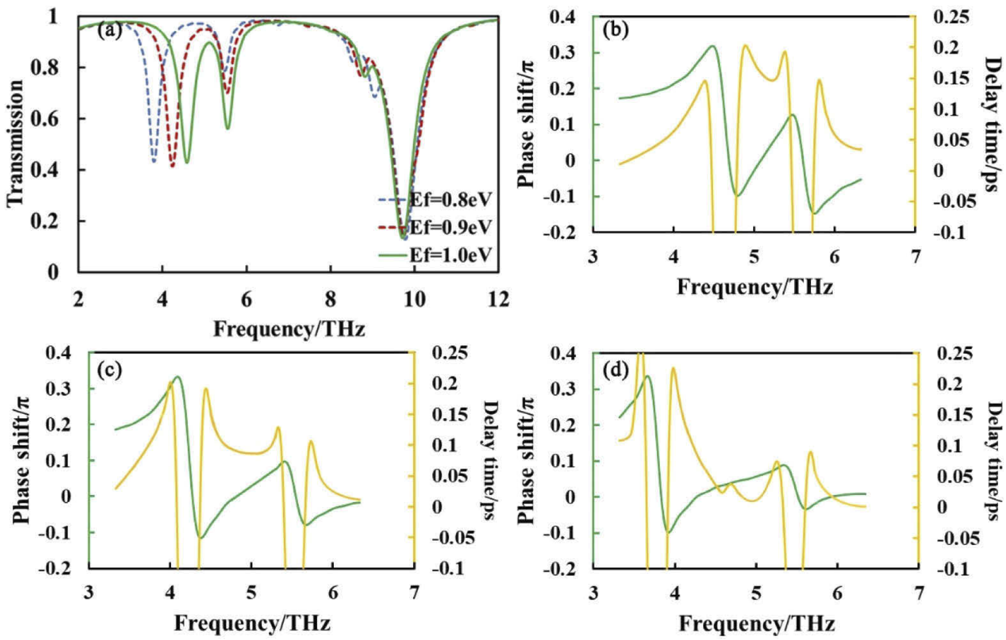

Fig. 7. (a) Transmission spectrum of tunable slow light at various Fermi levels of the graphene. Only changing the Fermi level of *G1* make the transparent window shift, the other parameters are as same as Fig. 1(A color version of this figure can be viewed online.) (b)-(d) Phase shift (green solid line) and Delay time (yellow solid line) of slow light at different Fermi level, (b) is *G1* at 1 eV, (c) is *G1* at 0.9 eV, and (d) is *G1* at 0.8 eV.

4. Conclusion

In conclusion, we have proposed a multifunction graphene-based metasurface which can realize the tunable filter and PIT by the SPPs of graphene in the terahertz. The results of FDTD show that some superior characteristics including the narrow filters, phase changing and sensitivity of refractive index. According to the tunable conductivity theory of graphene, we discuss the changes of transmission spectra in different function modes with Fermi levels. Using the CMT, we have demonstrated the bright and dark mode coupling which generate two transparency windows in the SPPs frequency of patterned graphene. In addition, we have put forward a concept of dual-channel optical switch based on our device. Therefore, this work offers an unprecedented design for combining multiple functions including switch, refractive index sensor and slow light on one device.

Funding

National Natural Science Foundation of China (60907003, 61805278); China Postdoctoral Science Foundation (2018M633704); National University of Defense Technology (JC13-02-13, ZK17-03-01); Natural Science Foundation of Hunan Province (13JJ3001); Program for New Century Excellent Talents in University (NCET-12-0142); Hunan Provincial Innovation Foundation for Postgraduate (CX20200039).

Disclosures

The authors declare that there are no conflicts of interest.

Optics EXPRESS

See Supplement 1 for supporting content.

References

1. J. Gu, R. Singh, X. Liu, X. Zhang, Y. Ma, S. Zhang, S. A. Maier, Z. Tian, A. K. Azad, H. T. Chen, A. J. Taylor, J. Han, and W. Zhang, "Active control of electromagnetically induced transparency analogue in terahertz metamaterials," Nat. Commun. **3**(1), 1151 (2012).
2. S. Zhang, D. A. Genov, Y. Wang, M. Liu, and X. Zhang, "Plasmon-induced transparency in metamaterials," Phys. Rev. Lett. **101**(4), 047401 (2008).
3. C. Liu, P. Liu, C. Yang, Y. Lin, and H. Liu, "Analogue of dual-controlled electromagnetically induced transparency based on a graphene metamaterial," Carbon **142**, 354–362 (2019).
4. X. R. Jin, J. Park, H. Y. Zheng, S. Lee, Y. Lee, J. Y. Rhee, K. W. Kim, H. S. Cheong, and W. H. Jang, "Highly-dispersive transparency at optical frequencies in planar metamaterials based on two-bright-mode coupling," Opt. Express **19**(22), 21652–21657 (2011).
5. Z. Chen, J. Tao, J. Gu, J. Li, D. Hu, Q. Tan, F. Zhang, and X. Huang, "Tunable metamaterial-induced transparency with gate-controlled on-chip graphene metasurface," Opt. Express **24**(25), 29216 (2016).
6. N. Liu, S. Kaiser, and H. Giessen, "Magnetoinductive and electroinductive coupling in plasmonic metamaterial molecules," Adv. Mater. **20**(23), 4521–4525 (2008).
7. P. Tassin, L. Zhang, T. Koschny, E. N. Economou, and C. M. Soukoulis, "Low-loss metamaterials based on classical electromagnetically induced transparency," Phys. Rev. Lett. **102**(5), 053901 (2009).
8. N. Liu, L. Langguth, T. Weiss, J. Kästel, M. Fleischhauer, T. Pfau, and H. Giessen, "Plasmonic analogue of electromagnetically induced transparency at the Drude damping limit," Nat. Mater. **8**(9), 758–762 (2009).
9. X. R. Jin, Y. Lu, H. Zheng, Y. P. Lee, J. Y. Rhee, and W. H. Jang, "Plasmonic electromagnetically-induced transparency in symmetric structures," Opt. Express **18**(13), 13396 (2010).
10. Y. Lu, J. Y. Rhee, W. H. Jang, and Y. P. Lee, "Active manipulation of plasmonic electromagnetically-induced transparency based on magnetic plasmon resonance," Opt. Express **18**(20), 20912 (2010).
11. N. Chen, C. Liao, C. Chen, W. Fan, J. Wu, J. Li, S. Chen, B. Huang, and L. Lee, "Color-tunable mixed photoluminescence emission from Alq3 organic layer in metal-Alq3-metal surface plasmon structure[J]," Nanoscale Res. Lett. **9**(1), 569 (2014).
12. N. I. Landy, S. Sajuyigbe, J. J. Mock, D. R. Smith, and W. J. Padilla, "Perfect Metamaterial Absorber," Phys. Rev. Lett. **100**(20), 207402 (2008).
13. J. Wang, C. Fan, P. Ding, J. He, Y. Cheng, W. Hu, G. Cai, E. Liang, and Q. Xue, "Tunable broad-band perfect absorber by exciting of multiple plasmon resonances at optical frequency[J]," Opt. Express **20**(14), 14871 (2012).
14. N. Liu, M. Mesch, T. Weiss, M. Hentschel, and H. Giessen, "Infrared perfect absorber and its application as plasmonic sensor," Nano Lett. **10**(7), 2342–2348 (2010).
15. L. Lin and A. Roberts, "Light transmission through nanostructured metallic films: coupling between surface waves and localized resonances," Opt. Express **19**(3), 2626–2633 (2011).
16. W. L. Barnes, A. Dereux, and T. W. Ebbesen, "Surface plasmon subwavelength optics," Nature **424**(6950), 824–830 (2003).
17. F. Wang, Y. Zhang, C. Tian, C. Girit, A. Zettl, M. Crommie, and Y. R. Shen, "Gate-Variable optical transitions in graphene," Science **320**(5873), 206–209 (2008).
18. N. O. Weiss, H. Zhou, L. Liao, Y. Liu, S. Jiang, Y. Huang, and X. Duan, "Graphene: an emerging electronic material," Adv. Mater. **24**(43), 5782–5825 (2012).
19. A. Geim, "Science, Graphene: Status and Prospects," Science **324**(5934), 1530–1534 (2009).
20. X. Luo, Z. Q. Cheng, X. Zhai, Z. M. Liu, S. Q. Li, J. P. Liu, L. L. Wang, Q. Lin, and Y. H. Zhou, "A tunable dual-band and polarization-insensitive coherent perfect absorber based on double-layers graphene hybrid waveguide," Nanoscale Res. Lett. **14**(1), 337 (2019).
21. X. Luo, Z. M. Liu, L. L. Wang, J. P. Liu, and Q. Lin, "Tunable ultra-narrowband and wide-angle graphene-based perfect absorber in the optical communication region," Appl. Phys. Express **11**(10), 105102 (2018).
22. D. Chen, J. Yang, J. Zhang, J. Huang, and Z. Zhang, "Tunable broadband terahertz absorbers based on multiple layers of graphene ribbons[J]," Sci. Rep. **7**(1), 15836 (2017).
23. A. Y. Nikitin, F. Guinea, F. J. Garcia-Vidal, and L. Martin-Moreno, "Surface plasmon enhanced absorption and suppressed transmission in periodic arrays of graphene ribbons," Phys. Rev. B **85**(8), 081405 (2012).
24. Z. Fang, Y. Wang, A. Schlather, Z. Liu, P. M. Ajayan, G. F. J. de Abajo, P. Nordlander, X. Zhu, and N. J. Halas, "Active tunable absorption enhancement with graphene nanodisk arrays," Nano Lett. **14**(1), 299–304 (2014).
25. Z. Fang, S. Thongrattanasiri, A. Schlather, Z. Liu, L. Ma, Y. Wang, P. M. Ajayan, P. Nordlander, N. J. Halas, and G. F. J. de Abajo, "Gated Tunability and Hybridization of Localized Plasmons in Nanostructured Graphene," ACS Nano **7**(3), 2388–2395 (2013).
26. D. Chen, J. Yang, J. Huang, W. Bai, J. Zhang, S. Xu, and W. Xie, "The novel graphene metasurfaces based on split-ring resonators for tunable polarization switching and beam steering at terahertz frequencies," Carbon **154**, 350–356 (2019).

27. R. Degl'Innocenti, D. S. Jessop, Y. D. Shah, J. Sibik, J. A. Zeitler, P. R. Kidambi, S. Hofmann, H. E. Beere, and D. A. Ritchie, "Low-bias terahertz amplitude modulator based on split-ring resonators and graphene," ACS Nano **8**(3), 2548–2554 (2014).
28. X. He, X. Zhong, F. Lin, and W. Shi, "Investigation of graphene assisted tunable terahertz metamaterials absorber," Opt. Mater. Express **6**(2), 331 (2016).
29. Y. Zhao, B. Wu, B. Huang, and Q. Cheng, "Switchable broadband terahertz absorber/reflector enabled by hybrid graphene-gold metasurface," Opt. Express **25**(7), 7161 (2017).
30. J. Wang, C. Fan, J. He, P. Ding, E. Liang, and Q. Xue, "Double Fano resonances due to interplay of electric and magnetic plasmon modes in planar plasmonic structure with high sensing sensitivity," Opt. Express **21**(2), 2236–2244 (2013).
31. L. Wu, H. S. Chu, W. S. Koh, and E. P. Li, "Highly sensitive graphene biosensors based on surface plasmon resonance," Opt. Express **18**(14), 14395–14400 (2010).
32. L. Wang, X. Chen, A. Yu, Y. Zhang, J. Ding, and W. Lu, "Highly sensitive and wideband tunable terahertz response of plasma waves based on graphene field effect transistors," Sci. Rep. **4**(1), 5470 (2015).
33. R. Alaee, M. Farhat, C. Rockstuhl, and F. Lederer, "A perfect absorber made of a graphene micro-ribbon metamaterial," Opt. Express **20**(27), 28017–28024 (2012).
34. S. Thongrattanasiri, F. H. L. Koppens, and G. F. J. de Abajo, "Complete optical absorption in periodically patterned graphene," Phys. Rev. Lett. **108**(4), 047401 (2012).
35. M. Amin, M. Farhat, and H. Bağcı, "An ultra-broadband multilayered graphene absorber," Opt. Express **21**(24), 29938–29948 (2013).
36. S. Yi, M. Zhou, X. Shi, Q. Gan, J. Zi, and Z. Yu, "A multiple-resonator approach for broadband light absorption in a single layer of nanostructured graphene," Opt. Express **23**(8), 10081–10090 (2015).
37. B. Zhang, H. Li, H. Xu, M. Zhao, C. Xiong, C. Liu, and K. Wu, "Absorption and slow-light analysis based on tunable plasmon-induced transparency in patterned graphene metamaterial," Opt. Express **27**(3), 3598 (2019).
38. T. T. Kim, H. D. Kim, R. Zhao, S. S. Oh, T. Ha, D. S. Chung, Y. H. Lee, B. Min, and S. Zhang, "Electrically Tunable Slow Light Using Graphene Metamaterials," ACS Photonics **5**(5), 1800–1807 (2018).
39. M. D. Goldflam, I. Ruiz, S. W. Howell, J. R. Wendt, M. B. Sinclair, D. W. Peters, and T. E. Beechem, "Tunable dual-band graphene-based infrared reflectance filter," Opt. Express **26**(7), 8532 (2018).
40. Z. Wei, X. Li, J. Yin, R. Huang, Y. Liu, W. Wang, H. Liu, H. Meng, and R. Liang, "Active plasmonic band-stop filters based on graphene metamaterial at THz wavelengths," Opt. Express **24**(13), 14344 (2016).
41. M. M. Jadidi, A. B. Sushkov, R. L. Myers-Ward, A. K. Boyd, K. M. Daniels, D. K. Gaskill, M. S. Fuhrer, H. D. Drew, and T. E. Murphy, "Tunable terahertz hybrid metal-graphene plasmons," Nano Lett. **15**(10), 7099–7104 (2015).
42. W. Tang, L. Wang, X. Chen, C. Liu, A. Yu, and W. Lu, "Dynamic metamaterial based on the graphene split ring high-Q Fano-resonnator for sensing applications," Nanoscale **8**(33), 15196–15204 (2016).
43. M. S. Yang, L. J. Liang, Z. Zhang, Y. Xin, D. Q. Wei, X. X. Song, H. T. Zhang, Y. Y. Lu, M. Wang, M. J. Zhang, T. Wang, and J. Q. Yao, "Electromagnetically induced transparency-like metamaterials for detection of lung cancer cells," Opt. Express **27**(14), 19520–19529 (2019).
44. B. Xiao, S. Tong, A. Fuffe, and Z. Shi, "Tunable electromagnetically induced transparency based on graphene metamaterials," Opt. Express **28**(3), 4048–4057 (2020).
45. E. H. Hwang and S. D. Sarma, "Dielectric function, screening, and plasmons in two-dimensional graphene," Phys. Rev. B **75**(20), 205418 (2007).
46. H. Hu, X. Guo, D. Hu, Z. Sun, X. Yang, and Q. Dai, "Flexible and Electrically Tunable Plasmons in Graphene-Mica Heterostructures," Adv. Sci. **5**(8), 1800175 (2018).
47. C. Zeng, Y. Cui, and X. Liu, "Tunable multiple phase-coupled plasmon-induced transparencies in graphene metamaterials," Opt. Express **23**(1), 545–551 (2015).
48. H. Yan, T. Low, F. Guinea, F. Xia, and P. Avouris, "Tunable phonon-induced transparency in bilayer graphene nanoribbons," Nano Lett. **14**(8), 4581–4586 (2014).
49. S. X. Xia, X. Zhai, L. L. Wang, B. Sun, J. Q. Liu, and S. C. Wen, "Dynamically tunable plasmonically induced transparency in sinusoidally curved and planar graphene layers," Opt. Express **24**(16), 17886–17899 (2016).
50. J. Yang, X. He, Y. Han, D. Chen, J. Zhang, J. Huang, and Z. Zhang, "Ultra-compact beam splitter and filter based on a graphene plasmon waveguide," Appl. Opt. **56**(35), 9814–9821 (2017).
51. A. Yariv, "Coupled-mode theory for guided-wave optics," IEEE J. Quantum Electron. **9**(9), 919–933 (1973).
52. H. Xu, H. Li, Z. He, Z. Chen, M. Zheng, and M. Zhao, "Dual tunable plasmon-induced transparency based on silicon-air grating coupled graphene structure in terahertz metamaterial," Opt. Express **25**(17), 20780–20790 (2017).
53. X. Yan, M. Yang, Z. Zhang, L. Liang, D. Wei, M. Wang, M. Zhang, T. Wang, L. Liu, J. Xie, and J. Yao, "The terahertz electromagnetically induced transparency-like metamaterials for sensitive biosensors in the detection of cancer cells," Biosens. Bioelectron. **126**, 485–492 (2019).
54. Y. Qian, Y. Zhao, Q. Wu, and Y. Yang, "Review of salinity measurement technology based on optical fiber sensor," Sens. Actuators, B **260**, 86–105 (2018).
55. Z. Wei, X. Li, N. Zhong, X. Tan, X. Zhang, H. Liu, H. Meng, and R. Liang, "Analogue Electromagnetically Induced Transparency Based on Low-loss Metamaterial and its Application in Nanosensor and Slow-light Device," Plasmonics **12**(3), 641–647 (2017).

Optics EXPRESS

56. N. Liu, T. Weiss, M. Mesch, L. Langguth, U. Eigenthaler, M. Hirscher, C. Sonnichsen, and H. Giessen, "Planar metamaterial analogue of electromagnetically induced transparency for plasmonic sensing," Nano Lett. **10**(4), 1103–1107 (2010).
57. F. Cheng, X. Yang, and J. Gao, "Enhancing intensity and refractive index sensing capability with infrared plasmonic perfect absorbers," Opt. Lett. **39**(11), 3185–3188 (2014).
58. Y. Zhang, T. Li, B. Zeng, H. Zhang, H. Lv, X. Huang, W. Zhang, and A. K. Azad, "Graphene based tunable terahertz sensor with double Fano resonances," Nanoscale **7**(29), 12682–12688 (2015).
59. H. Lu, X. Liu, and D. Mao, "Plasmonic analog of electromagnetically induced transparency in multinanoresonator-coupled waveguide systems," Phys. Rev. A **85**(5), 053803 (2012).
60. S. Xia, X. Zhai, Y. Huang, J. Liu, L. Wang, and S. Wen, "Graphene Surface Plasmons With Dielectric Metasurfaces," J. Lightwave Technol. **35**(20), 4553–4558 (2017).
61. Z. Liu, E. Gao, Z. Zhang, H. Li, H. Xu, X. Zhang, X. Luo, and F. Zhou, "Dual-Mode On-to-Off Modulation of Plasmon-Induced Transparency and Coupling Effect in Patterned Graphene-Based Terahertz Metasurface," Nanoscale Res. Lett. **15**(1), 1–13 (2020).
62. S. Xia, X. Zhai, L. Wang, and S. Wen, "Plasmonically induced transparency in double-layered graphene nanoribbons," Photonics Res. **6**(7), 692–702 (2018).